Research Article

Muhammad Nasir Amin*, Suleman Ayub Khan*, Ahmed A. Alawi Al-Naghi, Enamur R. Latifee, Nawaf Alnawmasi, and Ahmed Farouk Deifalla

Low-carbon embodied alkali-activated materials for sustainable construction: A comparative study of single and ensemble learners

https://doi.org/10.1515/rams-2023-0162 received October 04, 2023; accepted December 14, 2023

Abstract: Popular and eco-friendly alkali-activated materials (AAMs) replace Portland cement concrete. Due to the considerable compositional variability of AAMs and the inability of established materials science methods to understand composition-performance relationships, accurate property forecasts have proved impossible. This study set out to develop AAM compressive strength (CS) evaluation machine learning (ML) models using techniques including extreme gradient boosting (XGB), bagging regressor (BR), and multi-layer perceptron neural network (MLPNN). Ten input variables were used with a large dataset of 676 points. Statistical and K-fold studies were also used to evaluate the developed models' correctness. XGB predicted the CS of AAM the best, followed by BR and MLPNN. The MLPNN and BR models had R^2 values of 0.80 and 0.90, respectively, whereas the XGB model had 0.94. Results from statistical analyses and k-fold cross-validation of the used ML models further attest to their validity. The built models can potentially compute the CS of AAMs for a variety of input parameter values, reducing the requirement for costly and time-consuming laboratory testing. Researchers and businesses may find this study useful in determining the necessary quantities of AAMs' raw components.

Keywords: alkali-activated materials, machine learning, compressive strength

Ahmed A. Alawi Al-Naghi, Enamur R. Latifee, Nawaf Alnawmasi: Civil Engineering Department, University of Ha'il, Ha'il 55476, Saudi Arabia Ahmed Farouk Deifalla: Department of Structural Engineering and Construction Management, Future University in Egypt, New Cairo City 11835, Egypt

1 Introduction

An estimated 5–8% of the world's total anthropogenic CO₂ emissions [1] come from ordinary Portland cement (OPC) manufacturing, and this number is expected to increase by 8% in 2050 under current projections [2], which questions whether or not the Paris Agreement's zero-emissions goal can be achieved. In order to reduce CO₂ emissions from the OPC business, it is crucial to find alternatives to OPC that are less harmful to the environment [3,4]. As a result of their low energy requirements and negative impact on the environment, alkali-activated materials (AAMs) have garnered interest as one of the most promising building materials during the past few decades [5,6]. Alkaline activators react with alumino-silicate resources (mining wastes, industrial by-products, and minerals) to produce AAMs [7,8]. Some of the alumino-silicates that can be used as building blocks in the production of AAM are described in previous studies [9-12] and include fly ash, blast furnace slag, met kaolin, red mud, and rice husk ashes, respectively. In order to acquire appropriate technical features at a reasonable cost, activators based on sodium have been widely used [13]. Sodium carbonate, water glass, and sodium hydroxide are all examples. Some large-scale construction projects have used AAMs; examples include offshore structures, houses, watertight buildings, and immobilizations of heavy metals [14]. A more general term for a wide range of precursors that have been activated by alkaline solutions is AAM [15]. One kind of AAM, called geopolymers, is made by polymerizing aluminosilicate minerals in an alkaline environment. This process makes the material more uniform and organized. When it comes to high-performance concrete, geopolymers are often used because of their unique and controlled polymerization mechanism, in contrast to AAMs, which cover a broader range of compositions and structures [7,16]. Although there are some obvious problems that need fixing, such as the tendency for cracking due to shrinking [17], as an alternative to OPC concrete, AAMs

^{*} Corresponding author: Muhammad Nasir Amin, Department of Civil and Environmental Engineering, College of Engineering, King Faisal University, Al-Ahsa 31982, Saudi Arabia, e-mail: mgadir@kfu.edu.sa

^{*} Corresponding author: Suleman Ayub Khan, Department of Civil Engineering, COMSATS University Islamabad, Abbottabad 22060, Pakistan, e-mail: sulemanayub@cuiatd.edu.pk

have proven to be highly effective. AAMs have several advantages, which are shown in Figure 1.

Compressive strength (CS) is the main topic of this study since it is a crucial performance indicator for structural materials. By using CS, models can be trained, and predictive analyses can be conducted efficiently, with a primary focus on structural integrity; hence, a lot of studies have been performed to determine how factors like water/ binder ratio (w/b), precursor type, activator dosage, and curing conditions affect it. For example, Yang et al. [18] examined the effects of changing the w/b on the mechanical characteristics of alkali-activated slag concrete based on Ca(OH)₂. They discovered that by decreasing the w/b, the CS increased at a pace analogous to that of OPC concrete. Most alkali activation plants employ either ground granulated blast furnace slag (GGBFS) or fly ash as their precursor. Xie et al. [19] studied the impact of fly ash and GGBFS on the mechanical strength of recycled aggregate alkali-activated geo-polymer concrete. CS was shown to increase with increasing GGBS/fly ash ratio. This result agrees with that of Puertas et al. [20], who found that increasing the slag fraction in NaOH-activated fly ash/slag blends increased the blends' CS. The limited range of building applications for AAMs may be traced back to a lack of understanding of the vital implications of the multiple parameters on their CS.

Altering the activator types and the relative amounts between them allows for fine-tuning of AAMs' mechanical properties. To better understand alkali activation, Turkish

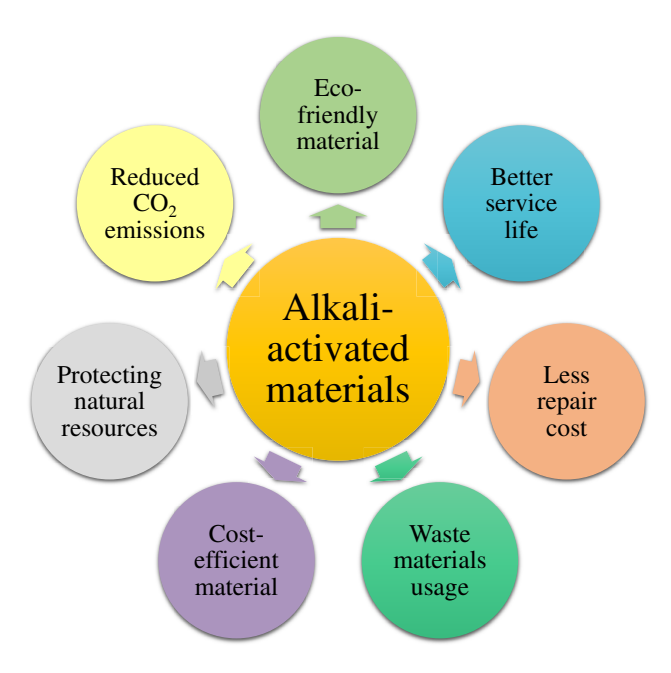


Figure 1: Advantages of AMMs.

slag's mechanical properties were studied by Aydın and Baradan [21], who looked into the effects of Na₂SiO₃ and NaOH activators. The test findings showed that the CS of the Na₂SiO₃₋activated slag mortars was more than that of the NaOH-activated specimens. CS was also shown to be highly dependent on the Na₂O content and the SiO₂/Na₂O ratio. Na₂SiO₃ and NaOH mortars, for instance, with SiO₂/ Na₂O ratio equal to 1.2 and Na₂O 8% of slag proportion, achieved the maximum CS after 28 days. Curing, the first step of geo-polymerization, is very sensitive to temperature. Rovnaník [22] examined the effects of the material's mechanical and microstructural properties at different curing temperatures (10, 20, 40, 60, and 80°C) on the geopolymer that was based on kaolin. The aforementioned parameters should be considered while planning the CS strength of AAM combinations. It used to take a lot of trial batches in the lab to get the right CS. However, it is a timeconsuming and costly operation to prepare many AAM specimens. Predictions of AAMs' CS without spending a lot of time and money on batch tests are better because they conserve resources and do not waste materials.

Soft computing approaches are quickly becoming the go-to for simulating the technical properties of different materials. To make informed forecasts, data-driven machine learning (ML) models are invaluable [23]. The complex design and inherent randomness of construction materials make accurate quality estimations challenging. ML techniques have been extensively used in estimating the engineering parameters of building materials. Materials such as self-compacting concrete, recycled aggregate concrete, fiber-reinforced concrete, PCM-integrated concrete, and lightweight concrete are some of the current and classic concretes whose properties have been studied using ML algorithms [24–28]. Numerous studies have shown that when estimating different concrete engineering qualities, robust ML models perform better than more conventional physical and empirical models. Some of the computational challenges in effectively forecasting concrete parameters [29–31] include cement paste's non-linear time and temperature-dependent performance and the intricate nature of cement hydration and microstructure development. On the other hand, input data on mixture proportions and curing conditions can be used to build ML models that can correctly predict the target attributes. ML models have various benefits, including the ability to make accurate and broad predictions, require less computation, and are easy to reproduce.

According to researched works, a trustworthy computational framework for predicting the CS of AAM composites may be established using well-trained ML algorithms. The current research aims to examine the CS of AAMs by employing a number of strong ML models. A data set

comprising 676 points has been compiled from research publications in the open literature. In order to forecast the CS of AAMs, regression models based on multi-layer perceptron neural network (MLPNN), bagging regressor (BR), and extreme gradient-boosting (XGB) were created. Arithmetical checks and K-fold analysis were conducted to ensure the validity of the models. The findings may have far-reaching consequences for the building sector as a whole due to the novel instruments and methodologies they provide for the controlled investigation of material properties with little to no human intervention.

2 Methods

2.1 Data sample

The Anaconda Navigator program performed all the Python codes for the models used in this investigation. The models used a data set of AAMs from Zhang et al. [32] to make predictions about CS. A total of 676 datasets were used for the model comparisons, 80% of the entire data was used to train the model, and 20% was utilized to test it. A k-fold validation technique was used to confirm the accuracy of the required models. Data preparation was employed to gather and arrange the data. There is a well-known obstacle to knowledge discovery from data, but effective data preparation for data mining can assist in overcoming it. The goal of data preparation is to simplify the data by removing clutter and unimportant information. The model was examined by means of regression and techniques for distributing errors. Ten variables, including fly ash (F-Ash), slag (S), coarse aggregate (CA), w/b, fine aggregate (FA), sodium hydroxide (SH), sodium silicate (SS), curing temperature (C-Temp), specimen age (S-Age), and relative humidity (RH), were taken into account to determine CS. Because of the profound effect they have on AAM concrete, these criteria were selected. Histograms are shown in Figure 2 to display the frequency dispersion of each variable. The dispersion of the variables that make up a dataset is a good indicator for its frequency distribution. Viewing the relative frequency distribution of a dataset reveals the prevalence of each value.

2.2 Modeling approaches

The CS of AAMs was assessed by actual trial techniques. The procedures took ten input parameters and returned only one output, i.e., CS. Anaconda Navigator scripts written in Python and Spyder (5.1.5) were employed to achieve the study's goals. Individual ML techniques, such as MLPNN, as well as ensemble ML techniques, such as BR and XGB, were employed to estimate the CS of AAMs. Applying ML algorithms to assess outputs in light of input features is a widespread practice. Only 20% of the data was actually used for testing, while 80% was used to train ML models. The R^2 of the expected result demonstrates the efficiency of the model employed. If the R^2 value is high, the predicted and observed values are very close, whereas if it is low, the disparity is substantial. Statistical testing, error valuations, and k-fold methods were also employed to confirm the model's correctness. Some of the statistics used in these evaluations included the mean absolute percentage error (MAPE), mean absolute error (MAE), and the root mean square error (RMSE). These parameters were chosen for ML model validation based on their effective usage in previous similar studies [33,34]. Figure 3 depicts the modeling of a sequence of events. The study's use of ML algorithms and validation strategies are discussed in the following sections.

2.2.1 MLPNN

The artificial neural network (ANN) is the most effective ML model available. It has been extensively used in ecological and hydrological engineering to deal with non-linear problems. The most popular ANN model is the MLPNN. Input, hidden, and output layers make up the MLPNN model's three-layer architecture. The three most frequent activation functions are logsig, purelin, and tansig. The output and hidden layers rely heavily on activations, bias functions, and weights. The model's weights or variables take on their final values during training. The hidden layers employ Tansig activation, whereas the output layer makes use of purelin. To get the best possible structure, the k-fold method is applied. In Figure 4, a generic neural network schematic chart is shown. In order to build one of these systems, one must first transmit the forward-pass input, then apply weight to it, and finally provide an estimate of the technique's output. Then, the calculated outputs are weighed against the factors that went into their creation. Predictions from the model take into account the inputs.

2.2.2 Bagging

The BR method is depicted in a simplified flowchart format in Figure 5. The incorporation of additional training data into the forecast model is primarily characterized by an

4 — Muhammad Nasir Amin et al. DE GRUYTER

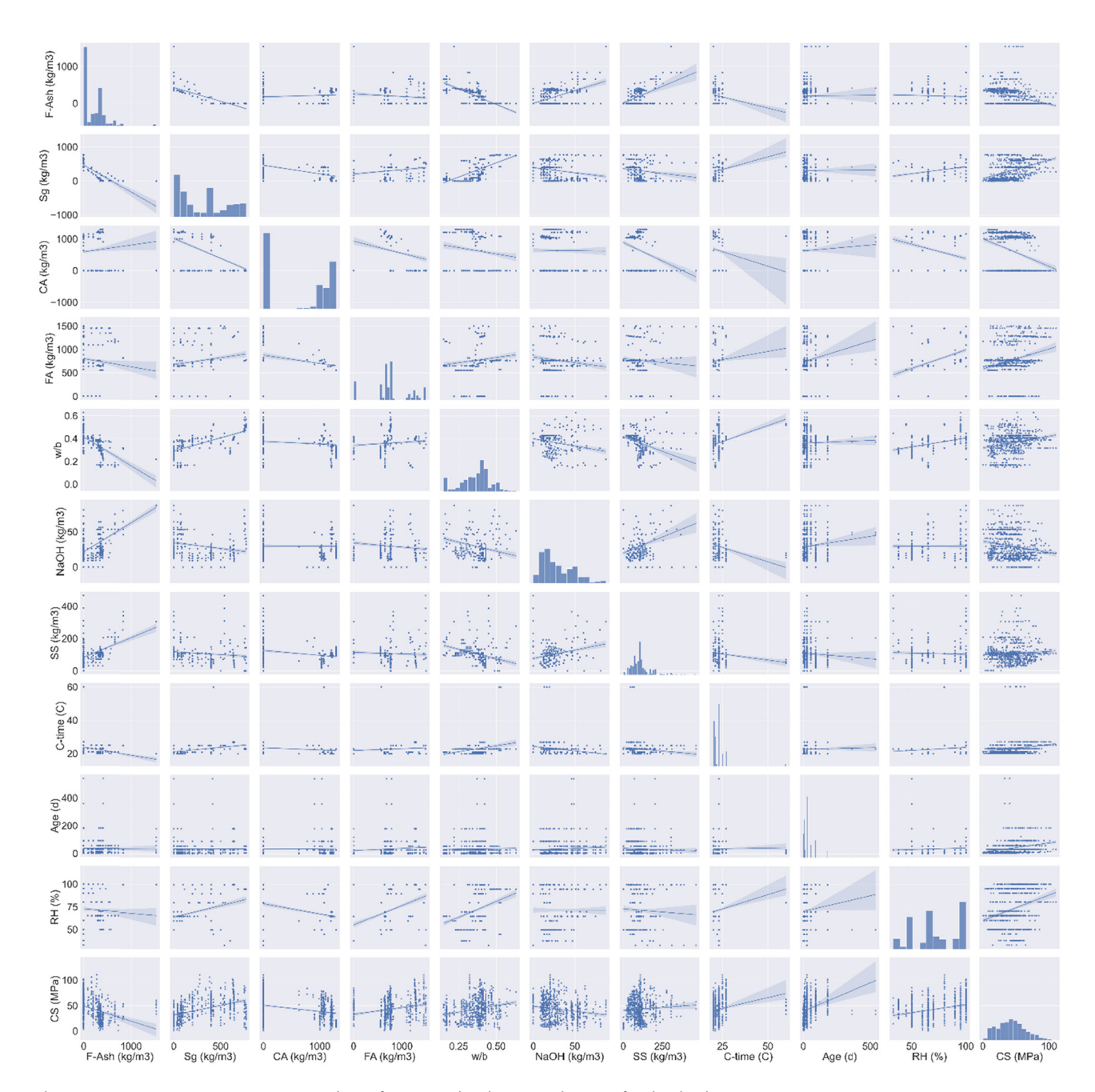


Figure 2: Variation in input parameters' relative frequency distribution and output for the database.

analogous ensemble method. Statistics from the original set are replaced with an asymmetrical sampling technique. If replacement sampling is used in training data, certain observations may be repeated in every new set. After bagging, each constituent has the same chance of appearing in the fresh data set. There is no correlation between the size of the training dataset and the projection quality. It is also possible that the divergence can be greatly decreased by improving the approximation of the target output. The average prediction across all simulations is used for this

ensemble. The average prediction from many simulations is used in regression [36]. The bagging method based on MLPNN is fine-tuned with the help of 20 sub-models to find the most productive output value.

2.2.3 XGB

Chen and Guestrin [38] created the XGB method, which is broadly renowned as a useful implement for data science

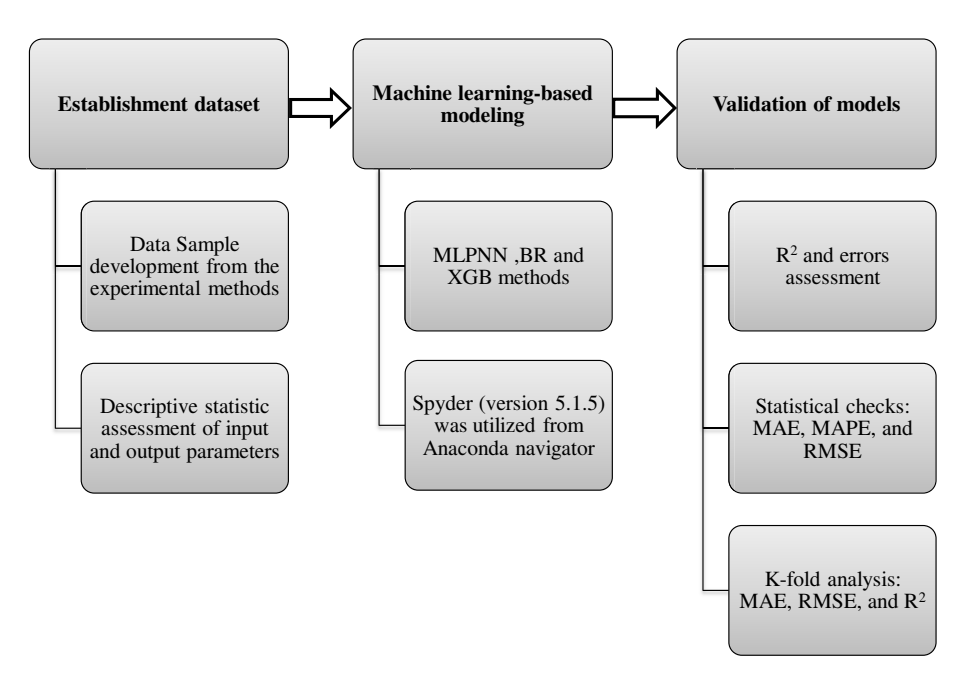


Figure 3: Flow diagram of data sample generation, modeling, and validation techniques.

investigators due to its tree-based collaborative learning approach. Utilizing many parameters to predict results in agreement with Eq. (1), the gradient boosting style forms the root of extreme gradient boosting (XGB) [39].

$$\bar{y_i} = y_i^0 + \eta \sum_{K=1}^n f_k(U_i).$$
 (1)

The "null" theory y_i^0 reflects the anticipated output; $\bar{y_i}$ with the ith figures and U_i as the restriction route signifies the expected output, reflects the pace of knowledge to improve a model's correctness and the joining of different trees to avoid excessive fitting, and signifies the estimator

magnitude in relation to different tree configurations in contrast to every f_k with k ranging from 1 to n. Creating models with little to no over-fitting is a major obstacle in ML. The XGB model employs supplementary assessments during its training phase.

Using the expected output $y_i^{-(k-1)}$ and the conforming shaped f_k subsequent to the kth identical forecaster given in Eq. (2), we can estimate y_i^{-k} at the kth level, as shown in Eq. (1).

$$y_i^{-k} = y_i^{-(k-1)} + \eta f_k.$$
 (2)

When the kth factual job of a tree is reduced, the resulting weight of the leaf is denoted by f_k (Eq. (3)):

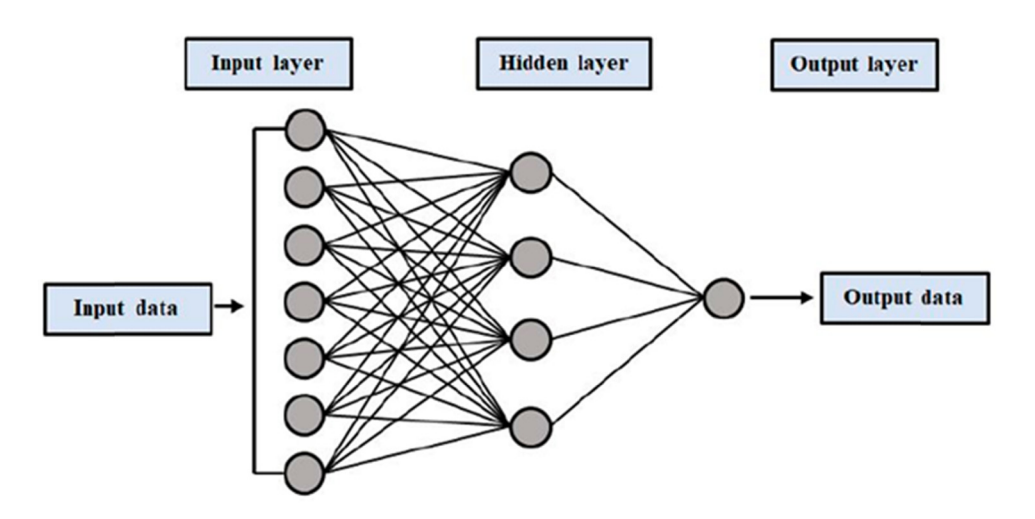


Figure 4: The MLPNN method depicted in a simplified diagram [35].

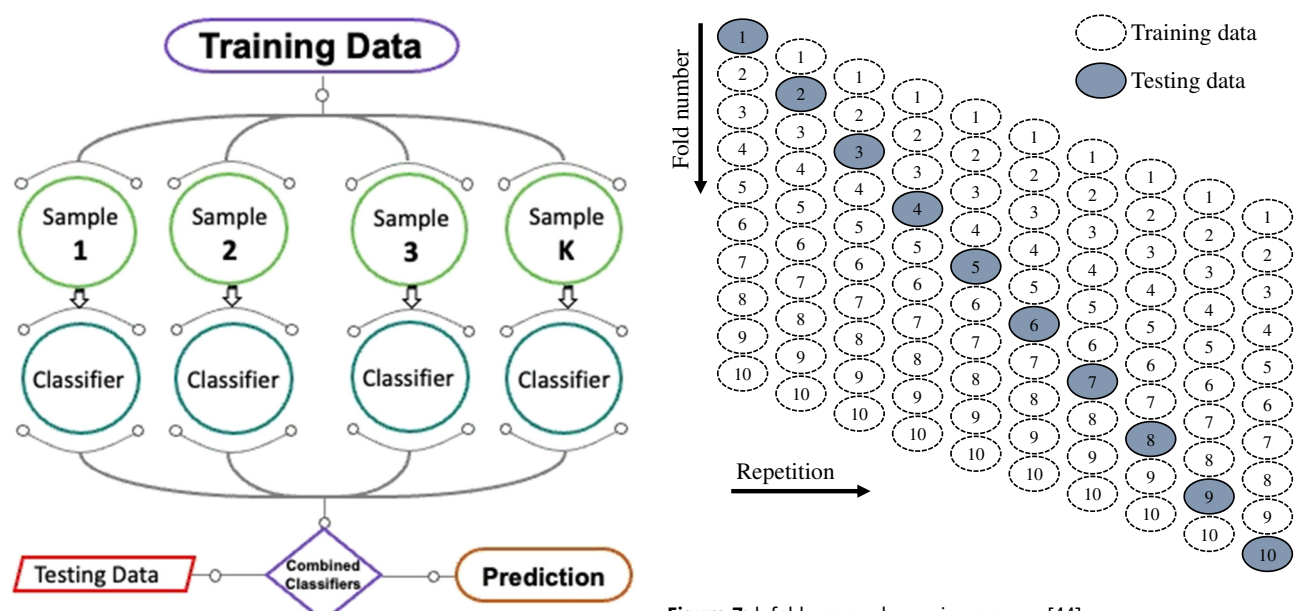


Figure 5: Schematic interpretation of the BR model [37].

$$f_{\text{obj}} = \gamma Z + \sum_{a=1}^{Z} \left[g_a \omega_a + \frac{1}{2} (h_a + \lambda) \omega_a^2 \right].$$
 (3)

Z denotes the section of leaf nodes, γ the complication aspect, λ the relentless factor, and ω_a^2 the leaf weight; λ and γ are the regulating factors employed to avoid excessive-fitting and expand the model. The loss of leaf gradient functions before and before the fact, denoted by h_a and

Figure 7: k-fold approach running process [44].

 g_a , respectively, are summed throughout the entire data sample. The kth tree can be made by slicing a single leaf into several smaller leaves. Eq. (4) illustrates the use of gain parameters in the implementation of such a system:

$$G = \frac{1}{2} \left[\frac{O_{\rm L}^2}{P_{\rm L} + \lambda} + \frac{O_{\rm R}^2}{P_{\rm R} + \lambda} + \frac{(O_{\rm L} + O_{\rm R})^2}{P_{\rm L} + P_{\rm R} + \lambda} \right],\tag{4}$$

 $P_{\rm R}$ and $O_{\rm R}$ and $P_{\rm L}$ and $O_{\rm L}$; where G denotes the gain variables, designate the right leaf. The gain parameter is

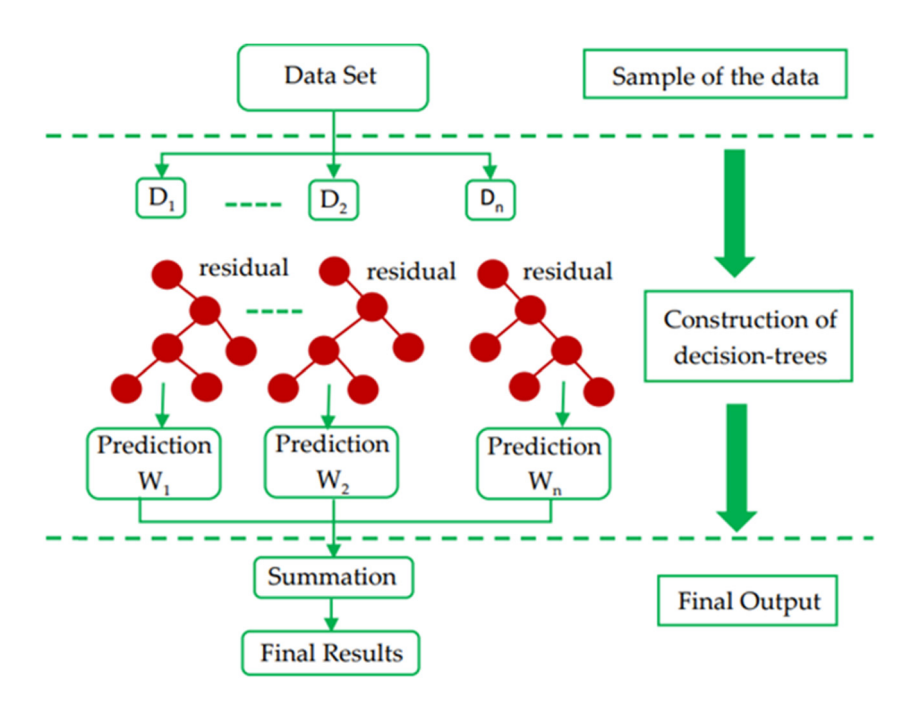
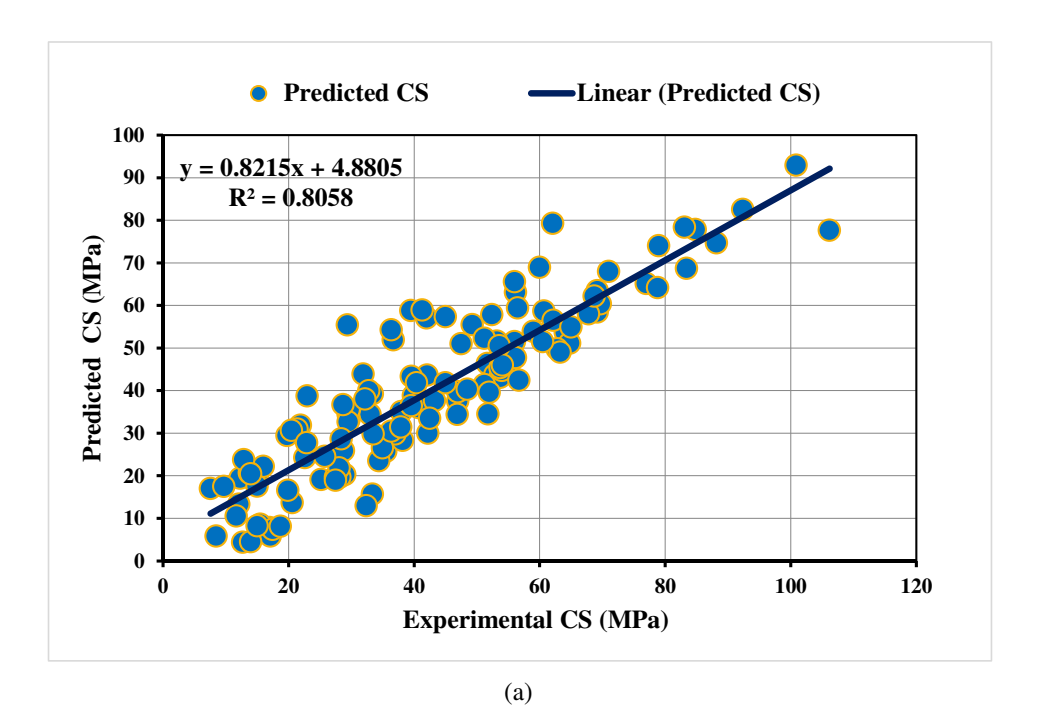


Figure 6: A simplified flowchart of the XGB method [40].

often rounded to zero, and the dividing line requirement is assumed. The gain regulates a regulating variable that acts meanderingly on the system. For example, the gain factor could be significantly lowered to stop the leaf convolution process by using a higher regularization value. However, doing so would diminish the model's performance on test data. Figure 6 depicts the fundamental hierarchy of the XGB tree algorithm.

2.2.4 Validation methods

The ML simulations were validated employing arithmetical methods and k-fold procedures. The k-fold strategy is frequently employed to evaluate a simulation's accuracy by arbitrarily splitting the dataset into ten distinct groups [41]. Figure 7 displays that out of the ten groups used, only one was used for testing ML models, and nine were used for



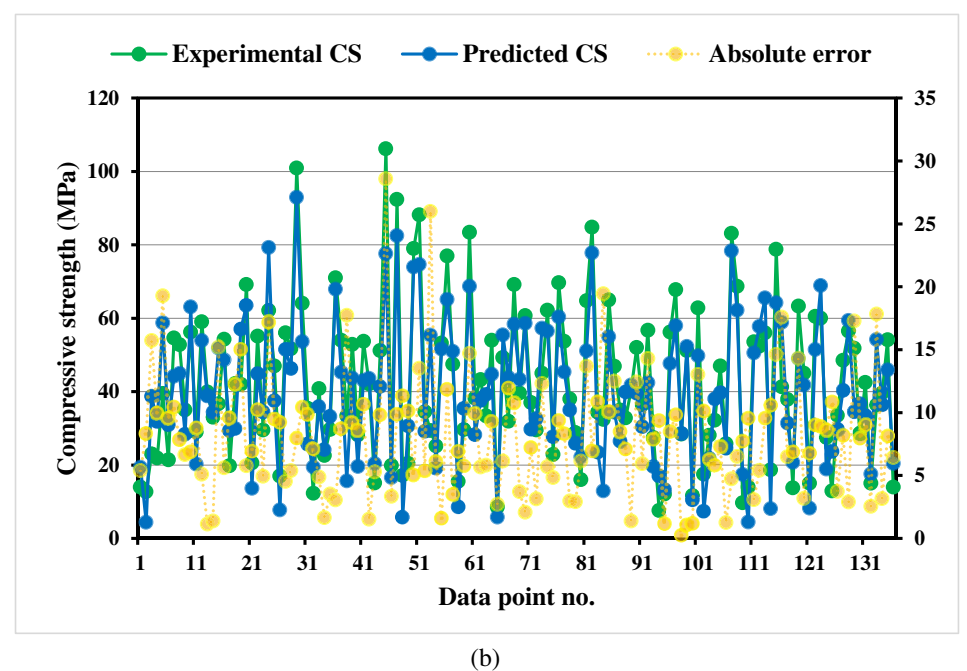
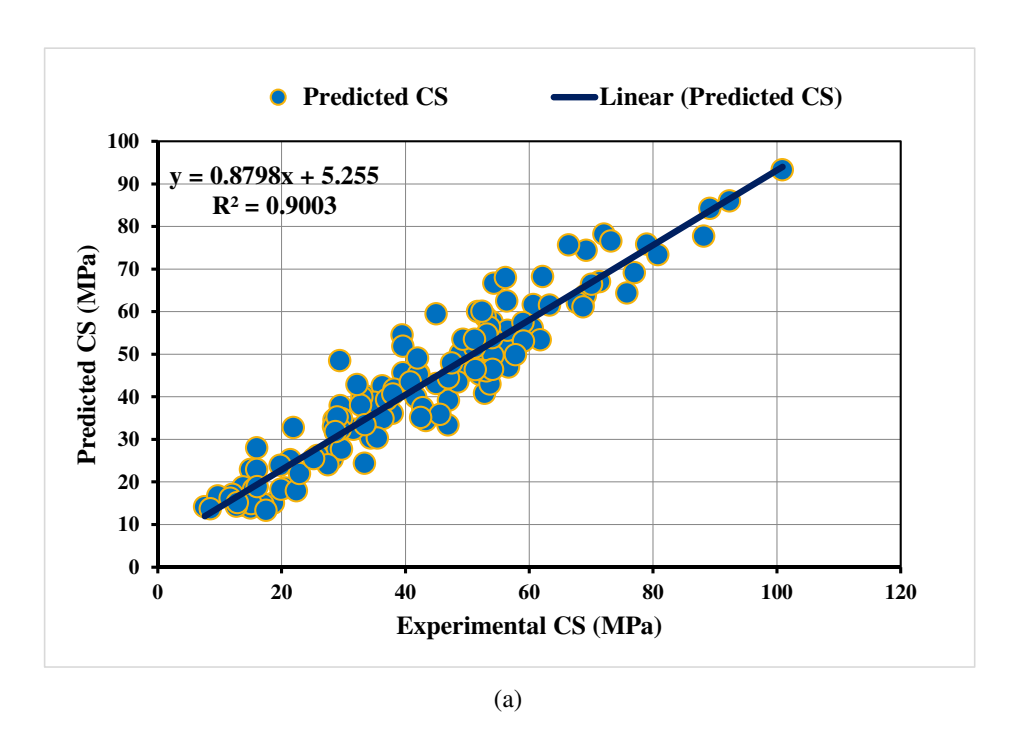


Figure 8: MLPNN-CS model: (a) correlation between observed and predicted results and (b) scattering of model outcomes, actual CS, and values of errors.

training. In cases where the error is minor and the \mathbb{R}^2 is large, the ML algorithm excels. In addition, repeating the process ten times is required to see the expected results. This technique considerably improves the model's already excellent accuracy. Statistical error estimation (MAPE, MAE, and RMSE) was also employed to scrutinize the precision of

various ML approaches. Using the acquired Eqs (5)–(7), we statistically checked the accuracy of the estimates from the ML techniques [42,43].

MAE =
$$\frac{1}{n} \sum_{i=1}^{n} |P_i - T_i|,$$
 (5)



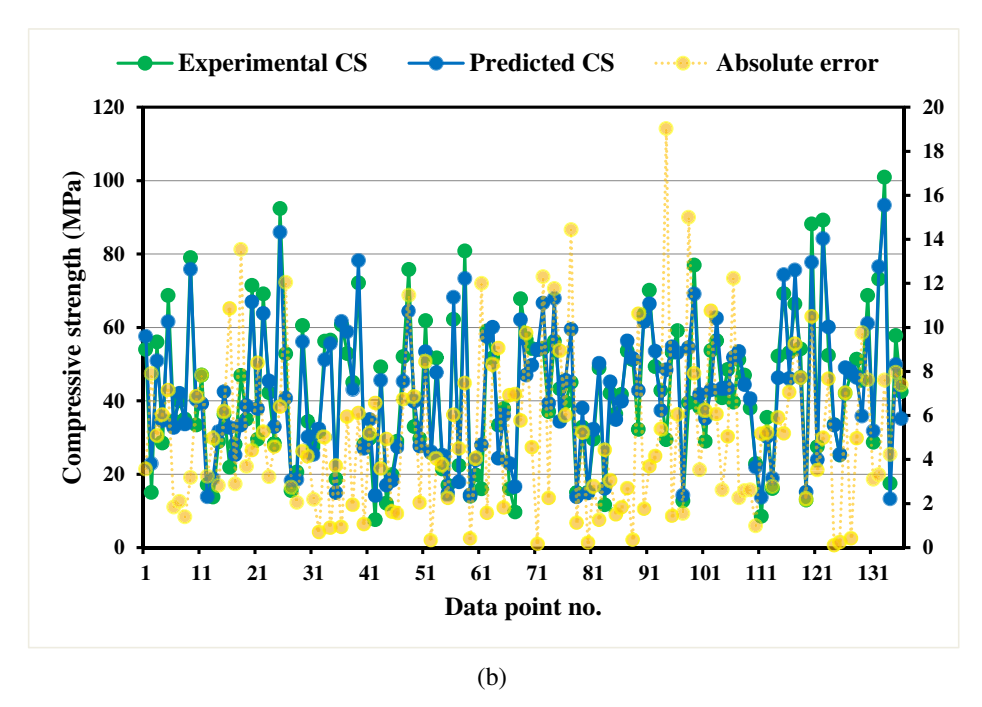


Figure 9: BR-CS model: (a) correlation between the observed and predicted results and (b) scattering of model outcomes, actual CS, and values of errors.

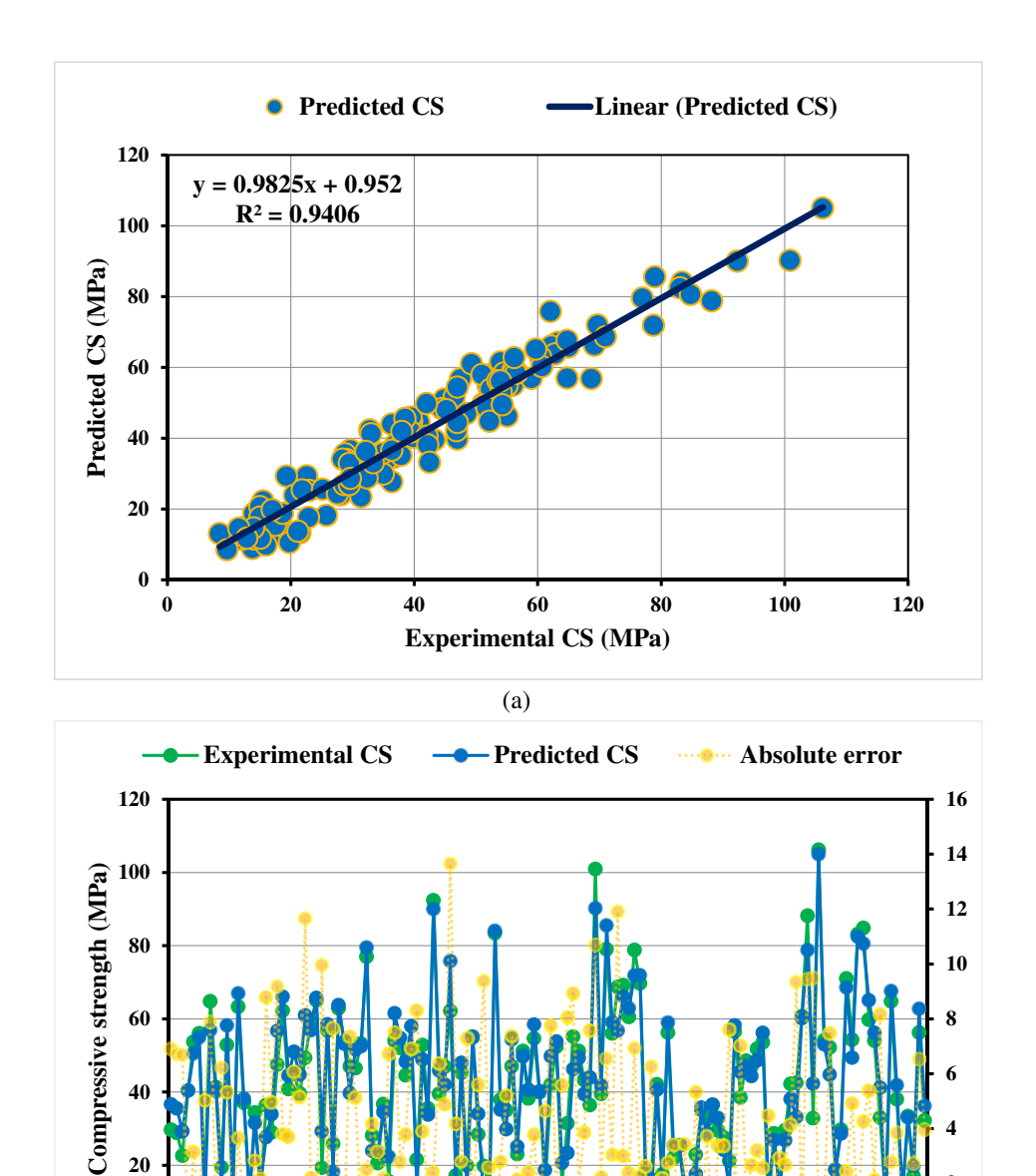


Figure 10: XGB-CS model: (a) correlation between the observed and predicted results and (b) scattering of model outcomes, actual CS, and values of errors.

(b)

61

71 81

Data point no.

91

$$RMSE = \sqrt{\sum \frac{(P_i - T_i)^2}{n}},$$

MAPE =
$$\frac{100\%}{n} \sum_{i=1}^{n} \frac{|P_i - T_i|}{T_i}$$
, (7)

21

31

41

51

where n is the statistics sample size, P_i is the projected outcome, and T_i is the actual value.

Table 1: Statistical analyses for assessing errors

101

111

121 131

ML method	MAE (MPa)	MAPE (%)	RMSE (MPa)
MLPNN	8.235	22.90	9.545
BR	5.140	15.20	6.239
XGB	4.125	10.70	5.064

3 Results and analysis

3.1 MLPNN model

Figure 8 displays the outcomes of using the MLPNN technique to estimate the CS of AAMs. Figure 8(a) shows the relationship between the estimated CS and the one that was tested. The MLPNN model predicted CS, however, with only a modest degree of accuracy and with significant variation between experimental and projected results. An R^2 of 0.80 shows a reasonable agreement between the actual and estimated outcomes, demonstrating that the MLPNN approach is useful for approximating the CS of AAMs. Figure 8(b) exhibits the experimental, expected, and error dispersion for the MLPNN method. The mean error value is 8.23 MPa, ranging between 0.25 and 28.57.32 MPa. Errors were also broken down proportionally, and it was found that out of all the strengths determined, just one was below 1 MPa, 31 were between 1 and 5 MPa, and 104 were above 5 MPa. The CS of AAMs was accurately forecasted using the MLPNN method, as evidenced by the dispersion of errors.

3.2 BR model

The outcomes of using the BR strategy to forecast the AAM's CS are shown in Figure 9. As displayed in Figure 9(a), there is an association between the actual and projected CS. The BR method produced the fewest discrepancies between the experimental and estimated outcomes, making it the preferred method above the MLPNN model utilized in the present study. The BR model seems to be more accurate due to

its R^2 of 0.90. The graphical representation of the BR technique's error dispersion for experimental, estimated, and deviating values is shown in Figure 9(b). The results showed that the lowest, median, and highest levels of errors were 0.12, 5.13, and 19.03 MPa. We examined how frequently different-sized errors occurred and discovered that 2% of them occurred at or below 1 MPa, 71% occurred between 1 and 5 MPa, and 63% occurred at or above 5 MPa. The error dispersion also shows that the BR model outperforms the MLPNN model in terms of precision. The BR method is more precise than the MLPNN model in determining the optimal output-producing value since it uses 20 sub-models to fine-tune the bagging method.

3.3 XGB model

The outcomes of using the XGB algorithm to forecast the CS of AAMs are displayed in Figure 10. The connection between the actual and predicted CS is presented in Figure 10(a). When comparing observed and anticipated results, the XGB approach turned out to be more precise. The XGB model's R^2 of 0.94 indicates its superior accuracy. The XGB method's distribution of actual, estimated, and error values is illustrated in Figure 10(b). The average deviation was found to be 4.12 MPa, with a maximum of 13.65 MPa. The distribution of the errors revealed that there were 18 values below 1 MPa, 71 values between 1 and 5 MPa, and 47 values exceeding 5 MPa. According to the error dispersion, the XGB technique outperformed the MLPNN and BR models. It is possible to deduce that the XGB approach is more precise than the MLPNN and BR in

Table 2: Outcomes of MAE, RMSE, and R^2 from the k-fold approach

k-fold number					CS (MPa)				
		MLPNN			BR			XGB	
	MAE	RMSE	R ²	MAE	RMSE	R ²	MAE	RMSE	R ²
1	10.86	13.98	0.71	10.46	12.91	0.64	10.14	17.71	0.68
2	11.59	10.81	0.68	7.58	8.49	0.71	10.06	12.63	0.70
3	9.79	14.83	0.56	11.12	13.99	0.64	7.08	10.73	0.76
4	10.28	16.31	0.22	12.52	16.70	0.57	9.65	10.26	0.39
5	13.71	27.53	0.80	11.90	22.76	0.90	7.28	11.76	0.77
6	15.47	14.38	0.17	13.27	15.74	0.25	10.56	15.43	0.29
7	10.26	15.41	0.78	10.71	12.88	0.68	6.64	7.84	0.93
8	8.67	13.87	0.58	11.79	14.63	0.38	8.81	14.65	0.33
9	16.30	16.41	0.15	11.31	16.51	0.48	10.21	16.73	0.67
10	12.06	9.89	0.73	9.69	12.40	0.62	8.00	9.94	0.64
Avg	11.90	15.34	0.54	11.04	14.70	0.59	8.84	12.77	0.62

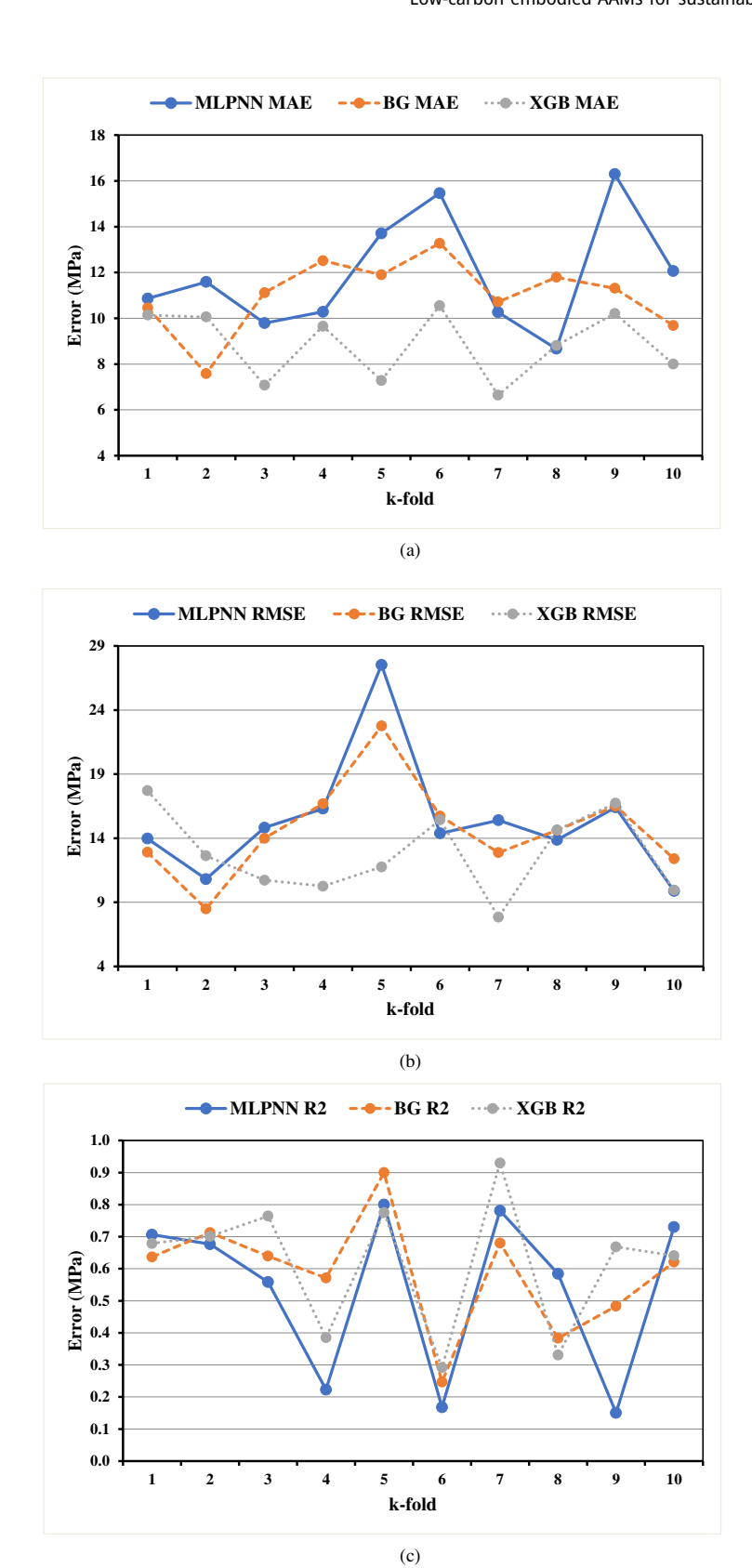


Figure 11: k-fold scrutiny results: (a) MAE, (b) RMSE, and (c) R^2 .

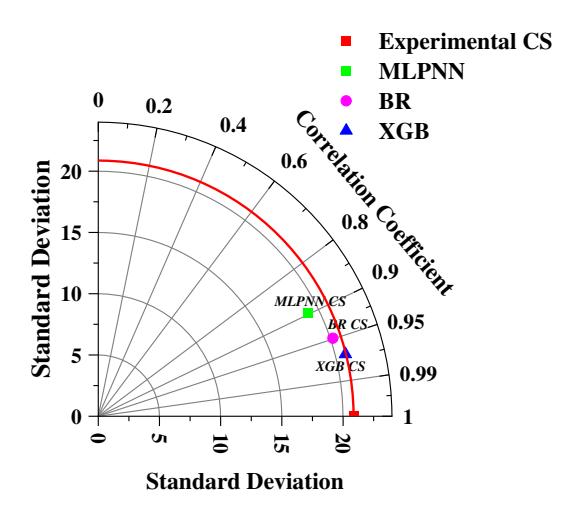


Figure 12: Taylor diagram for validation of models.

predicting the CS of AAMs. However, the MLPNN model's precision is very impressive. Accordingly, the CS of AAMs can be evaluated using any model, as all models showed significant prediction accuracy, as illustrated by the R^2 values and cross-validation techniques. The superior performance of XGB compared to other ML models is attributed to its gradient-boosting architecture that incorporates sophisticated features, such as regularization, parallel tree generation, and a proprietary loss function. By minimizing model complexity and resolving overfitting, XGB decreases bias and variance, resulting in higher predictive accuracy.

3.4 Model's validation

Using Eqs (5)–(7), the results from the error computations (RMSE, MAPE, and MAE) are shown in Table 1. It was found that the MLPNN, BR, and XGB all had MAE values of 8.235, 5.140, and 4.125 MPa, respectively, while predicting CS. MAPE was calculated to be 22.90% for MLPNN, 15.20% for BR, and 10.70% for XGB. Other results showed that RMSE values were 9.545 MPa for MLPNN, 6.239 MPa for BR, and 2.380 MPa for XGB. In comparison to the MLPNN and BR models, the XGB approach achieves a lower error rate, as

shown by these results. The validation scores for the k-fold approach, including R^2 , RMSE, and MAE, are displayed in Table 2. Figure 11 displays the outcomes of k-fold evaluations of several ML approaches to CS prediction. The MLPNN method produced a CS estimate with an MAE of 11.90 MPa, with a range of 8.67–16.30.75 MPa. The BR has an MAE of around 11.04 MPa on average, with a range of 7.58-13.27 MPa. Comparatively, the MAE for XGB ranged from 6.64 to 10.56 MPa, with a mean value of 8.84 MPa. The mean RMSEs for the MLPNN, BR, and XGB approaches were 15.34, 14.70, and 12.77 MPa, respectively. While BR and XGB have average R^2 values of 0.59 and 0.62. MLPNN's value is only 0.54. The finest XGB model for predicting the CS of AAMs has higher R^2 and lower errors. The increased accuracy of the XGB model was further validated by an analysis of these errors and R^2 values obtained utilizing the k-fold method. However, the accuracy of the MLPNN model is likewise satisfactory. Similarly, the Taylor diagram in Figure 12, which compares all of the forecasting models, served as validation. Therefore, it is possible that MLPNN, BR, and XGB models can be used to estimate the CS of AAMs more accurately.

4 Discussion

As the only binding material, OPC has a large global footprint in terms of both raw material depletion [45] and anthropogenic emissions [46]. Because of this, the OPC sector must find environmentally preferable replacements for OPC in order to reduce its $\rm CO_2$ emissions. AAMs have gained a great deal of attention over the past decade [47] as one of the most capable building materials due to their low environmental influence and energy depletion. AAM CS was estimated using MLPNN, BR, and XGB ML. To find the most accurate predictor, each approach was compared. XGB predicted CS more accurately than MLPNN and BR, with an R^2 of 0.94. MLPNN and BR had CS estimate R^2 of 0.80 and 0.90, respectively. The XGB approach's accuracy was further enhanced by the error gap between the actual

Table 3: Previous ML-based similar studies

Ref.	Technique	Material type	Property	Best model (<i>R</i> ² -value)
[49]	Ridge regression, RF, LightGBM, and XGB	Fly ash-slag based one-part AAM	CS	XGB (0.94)
[50]	Decision tree, RF, ANN, XGB	Concrete	Interface shear strength	XGB (0.94)
[51]	XGB	Asphalt concrete mixture	Dynamic modulus	XGB (0.96)
[52]	BRegressor, ETRegressor, NuSVR, ANNs, and XGBoost	Fiber-reinforced concrete, mortar, and rocks	Fracture toughness	XGB (0.92)

and forecasted outcomes. Error analysis demonstrates that XGB models match experiments and predictions better than MLPNN and BR models. Previous studies have demonstrated that the XGB approach outperforms the individual ML methods when it comes to assessing the strength of the building materials [42,48], which is illustrated in Table 3.

The accuracy of ML methods was also assessed using both arithmetic and k-fold processes. Increases in \mathbb{R}^2 and decreases in MAE, RMSE, and MAPE indicate that a model is more accurate. The finest ML approach for predicting attributes in different study areas might, however, be difficult to define and suggest because algorithm performance is chiefly reliant on the amount of variables and dataset engaged [42]. Sub-models trained on the database and finetuned to increase accuracy are typically created using the weak learner in ensemble ML approaches. The R^2 dispersion for the XGB-CS sub-models is 0.62 on average, with values between 0.29 and 0.93. According to these findings, XGB-CS sub-models outperform MLPNN and BR models in terms of accuracy. Thus, adopting AAMs instead of OPCbased composites will produce better construction materials with equivalent strength. More importantly, it will lessen OPC production's environmental impact and control its depletion of raw supplies.

The current study estimated CS utilizing 676 data records. These predictions considered ten variables. Future studies could add experimental data to improve model accuracy. By expanding the dataset, the model can make more accurate predictions. This study also used individual and ensemble ML models. However, hybrid ML methods like GA-PSO, Multi-Expression Programming, and RF-ANN, as well as individual/standalone and ensemble algorithms like SVM, DT, and boosting, could be studied in the future. These hybrid strategies can boost model performance and prediction; hence, they should be used. This study did not apply the sensitivity approach, LIME (local interpretable model-agnostic explanations), or PDP (partial dependence plots), but they can be used to explain the ML model's prediction. Mechanical qualities have been the primary focus of the existing literature on using ML approaches to the prediction of AAM's parameters. The microstructure, dynamic properties (fatigue), and longevity of AAMs have been the subject of a few investigations. Further research is required to thoroughly examine these aspects affecting durability using ML approaches.

5 Conclusions

This study created the CS of ML models to predict AAMs. A vast dataset of 676 experimental integrating combinations

was collected from scholarly literature. The CS of AAM was predicted using ML models, such as MLPNN, BR, and XGB. The statistical parameters and k-fold analysis examined the developed model's prediction accuracy. The study findings are summarized as follows:

- MLPNN and BR methods had a sufficient level of precision, with R^2 of 0.80 and 0.90, respectively, though the XGB method had a superior level of correctness, with R^2 of 0.94, for CS estimation.
- The difference between the experimental and estimated CS (errors) in the MLPNN, BR, and XGB techniques, on average, was 8.23, 5.14, and 4.12 MPa, respectively. These error values also supported MLPNN and BR models' appropriate accuracy, while the XGB method had a greater precision in predicting the strength of AAMs.
- The efficiency of the built models was proven by statistical evaluations. Better R^2 and lower errors indicated the accuracy of ML models. For the CS prediction in the MLPNN, BR, and XGB models, the MAPE values were found to be 22.00, 15.20, and 10.70%, respectively. The MAPE results supported the XGB model's superior ability to forecast the CS of AAMs.
- The XGB model outperforms the MLPNN and bagging models in terms of performance towards the intended outcome, as confirmed by the k-fold validation approach.

The findings of this study shed new light on the design of AAMs based on the robust prediction frameworks established here. Scientists and engineers can benefit from the study's methods by more easily assessing, improving, and rationalizing the mixture proportioning of AAMs. The assistance that ML models offer in mixture design encourages sustainable building and reduces the environmental challenges of the conventional concrete industry.

Acknowledgments: The authors would like to express their deepest gratitude to the Scientific Research Deanship and the College of Engineering at the University of Ha'il-Saudi Arabia for providing the necessary support for conducting this research through project number RG-23 062.

Funding information: This research was funded by the Scientific Research Deanship at the University of Ha'il, Saudi Arabia, through project number RG-23 062.

Author contributions: M.N.A.: conceptualization, project administration, funding acquisition, supervision, writing, reviewing, and editing. S.A.K.: conceptualization, data acquisition, software, methodology, supervision, and writing – original draft. A.A-N.: investigation, funding acquisition, resources, writing, reviewing, and editing. E.R.L.: formal

analysis, data acquisition, methodology, writing, reviewing, and editing. N.A: formal analysis, visualization, writing, reviewing, and editing. A.F.D.: validation, investigation, writing, reviewing, and editing. All authors have accepted responsibility for the entire content of this manuscript and approved its submission.

Conflict of interest: The authors state no conflict of interest.

Data availability statement: The datasets generated during and/or analyzed during the current study are available from the corresponding author on reasonable request.

References

- [1] Castro-Alonso, M. J., L. E. Montañez-Hernandez, M. A. Sanchez-Muñoz, M. R. Macias Franco, R. Narayanasamy, and N. Balagurusamy. Microbially induced calcium carbonate precipitation (MICP) and its potential in bioconcrete: microbiological and molecular concepts. Frontiers in Materials, Vol. 6, 2019, id. 126.
- [2] Habert, G., S. A. Miller, V. M. John, J. L. Provis, A. Favier, A. Horvath, et al. Environmental impacts and decarbonization strategies in the cement and concrete industries. *Nature Reviews Earth & Environment*, Vol. 1, No. 11, 2020, pp. 559–573.
- [3] Poudyal, L. and K. Adhikari. Environmental sustainability in cement industry: An integrated approach for green and economical cement production. *Resources, Environment and Sustainability*, Vol. 4, 2021, id. 100024.
- [4] Khan, M. and C. McNally. A holistic review on the contribution of civil engineers for driving sustainable concrete construction in the built environment. *Developments in the Built Environment*, Vol. 16, 2023, id. 100273.
- [5] Nazar, S., J. Yang, M. N. Amin, M. Husnain, F. Ahmad, H. Alabduljabbar, et al. Investigating the influence of PVA and PP fibers on the mechanical, durability, and microstructural properties of one-part alkali-activated mortar: An experimental study. *Journal of Materials Research and Technology*, Vol. 25, 2023, pp. 3482–3495.
- [6] Nazar, S., J. Yang, M. Ashraf, F. Aslam, M. F. Javed, S. M. Eldin, et al. Formulation and characterization of cleaner one-part novel fly ash/ lime-based alkali-activated material. *Journal of Materials Research* and Technology, Vol. 23, 2023, pp. 3821–3839.
- [7] Gökçe, H. S., M. Tuyan, and M. L. Nehdi. Alkali-activated and geopolymer materials developed using innovative manufacturing techniques: A critical review. *Construction and Building Materials*, Vol. 303, 2021, id. 124483.
- [8] Riaz Ahmad, M., M. Khan, A. Wang, Z. Zhang, and J.-G. Dai. Alkaliactivated materials partially activated using flue gas residues: An insight into reaction products. *Construction and Building Materials*, Vol. 371, 2023, id. 130760.
- [9] Siddique, S. and J. G. Jang. Acid and sulfate resistance of seawater based alkali activated fly ash: A sustainable and durable approach. *Construction and Building Materials*, Vol. 281, 2021, id. 122601.
- [10] Kim, T. Characteristics of alkali-activated slag cement-based ultralightweight concrete with high-volume cenosphere. *Construction and Building Materials*, Vol. 302, 2021, id. 124165.

- [11] Sun, K., X. Peng, S. Wang, L. Zeng, P. Ran, and G. Ji. Effect of nano-SiO2 on the efflorescence of an alkali-activated metakaolin mortar. *Construction and Building Materials*, Vol. 253, 2020, id. 118952.
- [12] He, J., Y. Jie, J. Zhang, Y. Yu, and G. Zhang. Synthesis and characterization of red mud and rice husk ash-based geopolymer composites. *Cement and Concrete Composites*, Vol. 37, 2013, pp. 108–118.
- [13] Provis, J. L. and J. S. J. Van Deventer. Alkali activated materials: stateof-the-art report, RILEM TC 224-AAM, Springer Science & Business Media, Vol. 13, 2013.
- [14] Tian, X., F. Rao, R. Morales-Estrella, and S. Song. Effects of aluminum dosage on gel formation and heavy metal immobilization in alkali-activated municipal solid waste incineration fly ash. *Energy & Fuels*, Vol. 34, No. 4, 2020, pp. 4727–4733.
- [15] Ahmad, M. R., C. S. Das, M. Khan, and J.-G. Dai. Development of low-carbon alkali-activated materials solely activated by flue gas residues (FGR) waste from incineration plants. *Journal of Cleaner Production*, Vol. 397, 2023, id. 136597.
- [16] Nodehi, M. and V. M. Taghvaee. Alkali-activated materials and geopolymer: A review of common precursors and activators addressing circular economy. *Circular Economy and Sustainability*, Vol. 2, No. 1, 2022, pp. 165–196.
- [17] Kumarappa, D. B., S. Peethamparan, and M. Ngami. Autogenous shrinkage of alkali activated slag mortars: Basic mechanisms and mitigation methods. *Cement and Concrete Research*, Vol. 109, 2018, pp. 1–9.
- [18] Yang, K.-H., A.-R. Cho, and J.-K. Song. Effect of water–binder ratio on the mechanical properties of calcium hydroxide-based alkaliactivated slag concrete. *Construction and Building Materials*, Vol. 29, 2012, pp. 504–511.
- [19] Xie, J., J. Wang, R. Rao, C. Wang, and C. Fang. Effects of combined usage of GGBS and fly ash on workability and mechanical properties of alkali activated geopolymer concrete with recycled aggregate. *Composites Part B: Engineering*, Vol. 164, 2019, pp. 179–190.
- [20] Puertas, F., S. Martínez-Ramírez, S. Alonso, and T. Vázquez. Alkaliactivated fly ash/slag cements: Strength behaviour and hydration products. *Cement and concrete research*, Vol. 30, No. 10, 2000, pp. 1625–1632.
- [21] Aydın, S. and B. Baradan. Effect of activator type and content on properties of alkali-activated slag mortars. *Composites Part B: Engineering*, Vol. 57, 2014, pp. 166–172.
- [22] Rovnaník, P. Effect of curing temperature on the development of hard structure of metakaolin-based geopolymer. *Construction and building materials*, Vol. 24, No. 7, 2010, pp. 1176–1183.
- [23] Lao, J.-C., B.-T. Huang, L.-Y. Xu, M. Khan, Y. Fang, and J.-G. Dai. Seawater sea-sand engineered geopolymer composites (EGC) with high strength and high ductility. *Cement and Concrete Composites*, Vol. 138, 2023, id. 104998.
- [24] Marani, A., A. Jamali, and M. L. Nehdi. Predicting ultra-high-performance concrete compressive strength using tabular generative adversarial networks. *Materials*, Vol. 13, No. 21, 2020, id. 4757.
- [25] Marani, A. and M. L. Nehdi. Machine learning prediction of compressive strength for phase change materials integrated cementitious composites. *Construction and Building Materials*, Vol. 265, 2020, id. 120286.
- [26] Nunez, I., A. Marani, and M. L. Nehdi. Mixture optimization of recycled aggregate concrete using hybrid machine learning model. *Materials*, Vol. 13, No. 19, 2020, id. 4331.
- [27] Zhang, J., Y. Huang, F. Aslani, G. Ma, and B. Nener. A hybrid intelligent system for designing optimal proportions of recycled

- aggregate concrete. *Journal of Cleaner Production*, Vol. 273, 2020, id. 122922.
- [28] Zhang, J., D. Li, and Y. Wang. Toward intelligent construction: Prediction of mechanical properties of manufactured-sand concrete using tree-based models. *Journal of Cleaner Production*, Vol. 258, 2020, id. 120665.
- [29] Rajasekar, A., K. Arunachalam, and M. Kottaisamy. Assessment of strength and durability characteristics of copper slag incorporated ultra high strength concrete. *Journal of Cleaner Production*, Vol. 208, 2019, pp. 402–414.
- [30] Naseri, H., H. Jahanbakhsh, P. Hosseini, and F. M. Nejad. Designing sustainable concrete mixture by developing a new machine learning technique. *Journal of Cleaner Production*, Vol. 258, 2020, id. 120578.
- [31] Young, B. A., A. Hall, L. Pilon, P. Gupta, and G. Sant. Can the compressive strength of concrete be estimated from knowledge of the mixture proportions?: New insights from statistical analysis and machine learning methods. *Cement and Concrete Research*, Vol. 115, 2019, pp. 379–388.
- [32] Zhang, L. V., A. Marani, and M. L. Nehdi. Chemistry-informed machine learning prediction of compressive strength for alkaliactivated materials. *Construction and Building Materials*, Vol. 316, 2022. jd. 126103.
- [33] Ahmad, A., W. Ahmad, F. Aslam, and P. Joyklad. Compressive strength prediction of fly ash-based geopolymer concrete via advanced machine learning techniques. Case Studies in Construction Materials, Vol. 16, 2022, id. e00840.
- [34] Zou, B., Y. Wang, M. N. Amin, B. Iftikhar, K. Khan, M. Ali, et al. Artificial intelligence-based optimized models for predicting the slump and compressive strength of sustainable alkali-derived concrete. *Construction and Building Materials*, Vol. 409, 2023, id. 134092.
- [35] Nafees, A., S. Khan, M. F. Javed, R. Alrowais, A. M. Mohamed, A. Mohamed, et al. Forecasting the mechanical properties of plastic concrete employing experimental data using machine learning algorithms: DT, MLPNN, SVM, and RF. *Polymers*, Vol. 14, No. 8, 2022, id. 1583.
- [36] Huang, J., Y. Sun, and J. Zhang. Reduction of computational error by optimizing SVR kernel coefficients to simulate concrete compressive strength through the use of a human learning optimization algorithm. *Engineering with Computers*, Vol. 38, 2021, pp. 1–18.
- [37] Khan, K., W. Ahmad, M. N. Amin, A. Ahmad, S. Nazar, A. A. Alabdullah, et al. Exploring the use of waste marble powder in concrete and predicting its strength with different advanced algorithms. *Materials*, Vol. 15, No. 12, 2022, id. 4108.
- [38] Chen, T. and C. Guestrin, editors., Xgboost: A scalable tree boosting system, In Proceedings of the 22nd ACM SIGKDD International Conference on Knowledge Discovery and Data Mining (pp. 785–794), 2016.
- [39] Friedman, J. H. Greedy function approximation: a gradient boosting machine. *Annals of statistics*, Vol. 29, No. 5, 2001, pp. 1189–1232.
- [40] Amjad, M., I. Ahmad, M. Ahmad, P. Wróblewski, P. Kamiński, and U. Amjad. Prediction of pile bearing capacity using XGBoost algo-

- rithm: modeling and performance evaluation. *Applied Sciences*, Vol. 12, No. 4, 2022, id. 2126.
- [41] Ahmad, A., K. Chaiyasarn, F. Farooq, W. Ahmad, S. Suparp, and F. Aslam. Compressive strength prediction via gene expression programming (GEP) and artificial neural network (ANN) for concrete containing RCA. *Buildings*, Vol. 11, No. 8, 2021, id. 324.
- [42] Farooq, F., W. Ahmed, A. Akbar, F. Aslam, and R. Alyousef. Predictive modeling for sustainable high-performance concrete from industrial wastes: A comparison and optimization of models using ensemble learners. *Journal of Cleaner Production*, Vol. 292, 2021, id. 126032.
- [43] Aslam, F., F. Farooq, M. N. Amin, K. Khan, A. Waheed, A. Akbar, et al. Applications of gene expression programming for estimating compressive strength of high-strength concrete. *Advances in Civil Engineering*, Vol. 2020, 2020, pp. 1–23.
- [44] Khan, K., W. Ahmad, M. N. Amin, M. I. Rafiq, A. M. A. Arab, I. A. Alabdullah, et al. Evaluating the effectiveness of waste glass powder for the compressive strength improvement of cement mortar using experimental and machine learning methods. *Heliyon*, Vol. 9, No. 5, 2023, id. e16288.
- [45] Naqi, A. and J. G. Jang. Recent progress in green cement technology utilizing low-carbon emission fuels and raw materials: A review. Sustainability, Vol. 11, No. 2, 2019, id. 537.
- [46] Valente, M., M. Sambucci, M. Chougan, and S. H. Ghaffar. Reducing the emission of climate-altering substances in cementitious materials: A comparison between alkali-activated materials and Portland cement-based composites incorporating recycled tire rubber. *Journal of Cleaner Production*, Vol. 333, 2022, id. 130013.
- [47] Luukkonen, T., Z. Abdollahnejad, J. Yliniemi, P. Kinnunen, and M. Illikainen. One-part alkali-activated materials: A review. *Cement and Concrete Research*, Vol. 103, 2018, pp. 21–34.
- [48] Khan, K., W. Ahmad, M. N. Amin, A. Ahmad, S. Nazar, and M. A. Al-Faiad. Assessment of artificial intelligence strategies to estimate the strength of geopolymer composites and influence of input parameters. *Polymers*, Vol. 14, No. 12, 2022, id. 2509.
- [49] Shah, S. F. A., B. Chen, M. Zahid, and M. R. Ahmad. Compressive strength prediction of one-part alkali activated material enabled by interpretable machine learning. *Construction and Building Materials*, Vol. 360, 2022, id. 129534.
- [50] Xu, J.-G., S.-Z. Chen, W.-J. Xu, and Z.-S. Shen. Concrete-to-concrete interface shear strength prediction based on explainable extreme gradient boosting approach. *Construction and Building Materials*, Vol. 308, 2021, id. 125088.
- [51] Ali, Y., F. Hussain, M. Irfan, and A. S. Buller. An eXtreme Gradient Boosting model for predicting dynamic modulus of asphalt concrete mixtures. *Construction and Building Materials*, Vol. 295, 2021, id. 123642.
- [52] Dehestani, A., F. Kazemi, R. Abdi, and M. Nitka. Prediction of fracture toughness in fibre-reinforced concrete, mortar, and rocks using various machine learning techniques. *Engineering Fracture Mechanics*, Vol. 276, 2022, id. 108914.